Journal of Zhejiang University-SCIENCE A (Applied Physics & Engineering)
ISSN 1673-565X (Print); ISSN 1862-1775 (Online)
www.zju.edu.cn/jzus; www.springerlink.com
E-mail: jzus@zju.edu.cn

Syntheses and characterizations of alloyed $Co_xNi_{1-x}O$ nanocrystals*

Xin WANG[1], Zhi-zhen YE[†‡1], Yi-zheng JIN[†‡2]

([1]*State Key Laboratory of Silicon Materials, School of Materials Science and Engineering, Zhejiang University, Hangzhou 310027, China*)

([2]*Center for Chemistry of High-Performance and Novel Materials, State Key Laboratory of Silicon Materials, Department of Chemistry, Zhejiang University, Hangzhou 310027, China*)

[†]E-mail: yezz@zju.edu.cn; yizhengjin@zju.edu.cn

Received May 26, 2016; Revision accepted Sept. 25, 2016; Crosschecked Mar. 9, 2017

Abstract: Alloying is an effective way to manipulate the composition and physico-chemical properties of functional materials. We demonstrated the syntheses of alloyed $Co_xNi_{1-x}O$ nanocrystals using a nonaqueous approach, with x continuously tuned from 0 to 1 by varying the molar ratios of the cobalt precursor in the reagents. The morphological, structural, and compositional properties of the alloyed $Co_xNi_{1-x}O$ nanocrystals were characterized by transmission electron microscopy (TEM), X-ray diffraction (XRD), inductively coupled plasma atomic emission spectroscopy (ICP-AES), and energy dispersive X-ray spectroscopy (EDS). The results showed that the cobalt and nickel atoms were homogeneously distributed in the alloyed nanocrystals. The as-prepared $Co_xNi_{1-x}O$ nanocrystals can be applied as the hole-transporting layers in polymer light emitting diodes (PLEDs). Our study provides a good example for the syntheses of alloyed oxide nanocrystals with continuously tunable composition.

Key words: Alloying; Nickel oxide; Cobalt oxide; Colloidal nanocrystals
http://dx.doi.org/10.1631/jzus.A1600399 **CLC number:** O614.81

1 Introduction

Colloidal nanocrystals are an important class of functional materials because of the unique combination of solid state properties and excellent solution processability. The physico-chemical properties of colloidal nanocrystals highly rely on their composition, crystalline structure, and morphology. Alloying, which refers to the intended incorporation of foreign atoms into the matrix materials, provides an effective approach for controlling the composition of the colloidal nanocrystals (White *et al.*, 2008; Zhu *et al.*, 2008; Regulacio and Han, 2010).

NiO is an intrinsic p-type and wide bandgap semiconductor with high ionization potential and low electron affinity (Hüfner, 1994; Kılıç and Zunger, 2002; Yang *et al.*, 2011). Their unique electronic structure makes NiO nanocrystals attractive for a number of solution-processed optoelectronic devices (Liang *et al.*, 2014; Zhang J. *et al.*, 2014; Jiang *et al.*, 2015; Zhang H. *et al.*, 2016). Alloying may tailor the band structure of NiO nanocrystals to meet the requirements of various types of optoelectronics with different device structures and active materials. NiO has also been recognized as one of the most promising electrode materials for electrochemical applications (Lang *et al.*, 2008; Varghese *et al.*, 2008; Yuan *et al.*, 2009; Zhou *et al.*, 2012; Choi and Kang, 2014; Wang *et al.*, 2016; Xiao *et al.*, 2016; Zhang L.P. *et al.*, 2016). The alloyed compounds of NiO, for instance, single phased 3CoO·5NiO nanoparticles, exhibit better performance in lithium-ion batteries than that of those

‡ Corresponding authors
* Project supported by the National Natural Science Foundation of China (Nos. 91433204 and 51522209) and the Fundamental Research Funds for the Central Universities (No. 2015XZZX004-24), China
ORCID: Xin WANG, http://orcid.org/0000-0003-2171-8583

using the multiple phased patterns (e.g., NiO-Co_3O_4 hybrid nanocomposites) (Wang and Zhang, 2012).

Herein, we select colloidal $Co_xNi_{1-x}O$ nanocrystals as a model system to study the synthetic chemistry of alloyed oxide nanocrystals. NiO and CoO share the same rock salt structures and very close lattice parameters (0.41771 nm for NiO and 0.42667 nm for CoO), as well as similar radii of divalent metal ions (0.069 nm for Ni^{2+} and 0.065 nm for Co^{2+}). NiO-CoO solid solutions prepared by high-temperature (over 800 °C) calcination of bulk NiO and CoO have been explored by several studies (Stiglich *et al.*, 1973a; 1973b; Takizawa and Hagiwara, 2001; Kuboon and Hu, 2011). However, these NiO-CoO solid solutions are large-sized powders with poor colloidal solubility. Therefore, they cannot be utilized in solution-processed optoelectronic devices. In contrast, we aim to develop colloidal $Co_xNi_{1-x}O$ nanocrystals with excellent solubility. Our group previously developed a protecting-ligand assisted approach to prepare colloidal NiO nanocrystals (Liang *et al.*, 2014). In this study, we further extend the "ligand protection" approach to the syntheses of alloyed $Co_xNi_{1-x}O$ nanocrystals.

2 Methods

2.1 Materials

Nickel stearate ($Ni(St)_2$), lithium stearate (LiSt), and 1-octadecanol (ODA, 97%) were purchased from Alfa Aesar, UK. 1-octadecene (ODE, tech 90%) was purchased from Acros Organics, Belgium. Cobalt stearate ($Co(St)_2$, Co 9%–10%) was purchased from J&K Scientific, China. Hexane, methanol, ethyl acetate, and chloroform were analytical grade reagents (Sinopharm Chemical Reagent Co., Ltd., China). All chemicals were used as received.

2.2 Syntheses of alloyed $Co_xNi_{1-x}O$ nanocrystals

The syntheses of alloyed $Co_xNi_{1-x}O$ nanocrystals were conducted using standard Schlenk-line based technology. $Ni(St)_2$ and $Co(St)_2$ were selected as the nickel precursor and cobalt precursor, respectively. For simplicity, all the reactions were named after the molar ratio of the cobalt precursor. For a typical 20% (molar ratio) $Co(St)_2$ reaction, 0.4 mmol of $Ni(St)_2$, 0.1 mmol of $Co(St)_2$, 0.2 mmol of LiSt, 3 mmol of ODA, and 5 ml of ODE were loaded into a 25 ml three-necked flask. The mixture was heated to 100 °C and degassed for 1 h. The alcoholysis reaction was initiated by raising the temperature to 270 °C. The reaction solution was stabilized at this temperature for 1 h. For the 0, 40%, 60%, 80%, and 100% (molar ratio) $Co(St)_2$ reactions, the total amount of $Ni(St)_2$ and $Co(St)_2$ was kept at 0.5 mmol with varied concentrations of $Co(St)_2$ in the cationic precursors. The reaction solutions of the $Co_xNi_{1-x}O$ nanocrystals turned from brown to purple as the molar ratio of $Co(St)_2$ increased.

A two-step purification process was applied. The reaction solution was extracted four times using hexane/methanol mixtures at 50 °C to remove the residual metal carboxylates and ODA. Then, the products were precipitated by ethyl acetate and methanol. The resulting $Co_xNi_{1-x}O$ nanocrystals can be re-dispersed in non-polar solvents, such as hexane and chloroform. The nanocrystal solutions are stable for at least two months.

2.3 Fabrication of polymer light emitting diode

Indium tin oxide (ITO)-coated glass substrates were cleaned by ultrasonication in acetone, deionized water, and ethanol for 20 min, each, followed by oxygen-plasma treatment for 10 min. Then the $Co_xNi_{1-x}O$ film was deposited by spin-coating the nanocrystal solution at 4000 r/min, followed by annealing at 150 °C for 30 min in air and UV-ozone treatment. An m-xylene solution of poly[2-methoxy-5-(2-ethylhexyloxy)-1,4-phenylenevinylene] (MEH-PPV) (6 mg/ml) was spin-coated onto the $Co_xNi_{1-x}O$ nanocrystal thin films. Bi-layer top electrodes of Ca/Al (10 nm/100 nm) were deposited by thermal evaporation under a base pressure of 6×10^{-7} Torr. The device area was 1.44 mm^2 defined by the overlapping of the ITO and top electrodes.

2.4 Characterizations

The morphologies of alloyed $Co_xNi_{1-x}O$ nanocrystals were observed using transmission electron microscopy (TEM, JEOL JEM 1230, operated at 80 keV) and high-resolution TEM (HRTEM, JEM-2100F, operated at 200 keV). The crystal structures were measured by an X'Pert PRO system operated at 40 keV and 40 mA with Cu Kα radiation (λ=0.15406 nm). The content of cobalt in the $Co_xNi_{1-x}O$

nanocrystals was examined by inductively coupled plasma atomic emission spectroscopy (ICP-AES, IRIS Intrepid II XSP). The spherical-aberration (Cs) corrected scanning TEM under high-angle annular dark-field condition (HAADF-STEM) was performed by a Cs-corrected FEI Titan Chemi-STEM operated at 200 kV, with a Bruker SuperX energy dispersive X-ray spectroscopy (EDS) system for elementary mapping of a single nanoparticle. X-ray photoelectron spectroscopy (XPS, Thermo ESCALAB-250Xi, using Al Kα radiation as the X-ray source) was adopted to analyze the chemical state of Ni and Co elements.

For the polymer light emitting diode (PLED) characterizations, we used a Keithley 2400 electrometer for electrical measurements and a fiber integration sphere (FOIS-1) coupled with a QE-6500 spectrometer for light-output measurements (Dai *et al.*, 2014).

3 Results and discussion

Alloyed $Co_xNi_{1-x}O$ nanocrystals were prepared using the "ligand protection" approach. In this method, LiSt, which is inert in the reaction system, can bind onto the surface of oxide nanocrystals to reduce their reactivity and avoid the *in situ* reduction reactions (Liang *et al.*, 2014). Similar to the syntheses of pure NiO nanocrystals, metallic Ni particles formed in the syntheses of alloyed $Co_xNi_{1-x}O$ nanocrystals, if no protecting ligand of LiSt was introduced (data not shown).

We found that the morphology of the alloyed $Co_xNi_{1-x}O$ nanocrystals varied with the molar ratios of $Co(St)_2$ in the reagents (Fig. 1). Pure NiO nanocrystals are typical clusters consisting of several small particles with diameters of 2−3 nm. HRTEM observations (Fig. 2a) show that each primary particle is an irregular-shaped single crystal. The alloyed nanocrystals from the 20%, 40%, and 60% $Co(St)_2$ reactions are V-shaped nanostructures with short branches. These V-shaped nanostructures also exhibit a single-crystalline nature, as confirmed by HRTEM analyses. An image of a $Co_xNi_{1-x}O$ nanoparticle from the 60% $Co(St)_2$ reaction is shown in Fig. 2b. The $Co_xNi_{1-x}O$ nanocrystals from the 80% $Co(St)_2$ reaction are the mixture of V-shaped nanostructures and irregular nanoparticles. When the molar ratio of $Co(St)_2$ in the precursors rises to 100%, all the resulting nanocrystals are isolated particles with larger average diameters of about 8 nm. Note that similar phenomena, i.e., doping-/alloying-induced shape evolutions of colloidal nanocrystals, have also been

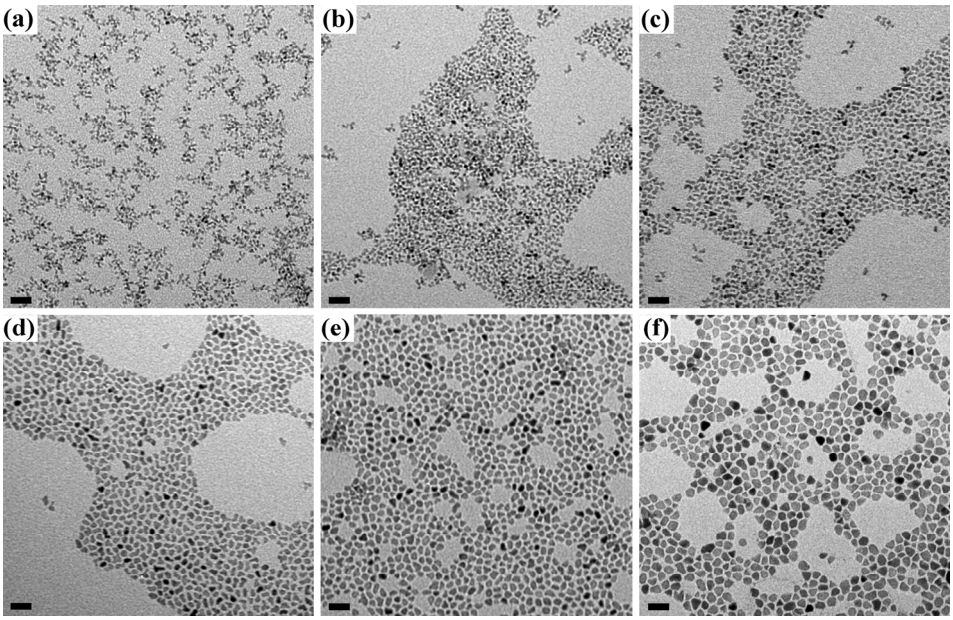

Fig. 1 Shape evolution of alloyed $Co_xNi_{1-x}O$ nanocrystals induced by increasing the molar ratio of $Co(St)_2$ in the cationic precursors: (a–f) TEM images of the alloyed $Co_xNi_{1-x}O$ nanocrystals from the 0, 20%, 40%, 60%, 80%, and 100% (molar ratio) $Co(St)_2$ reactions, respectively (scale bar: 20 nm)

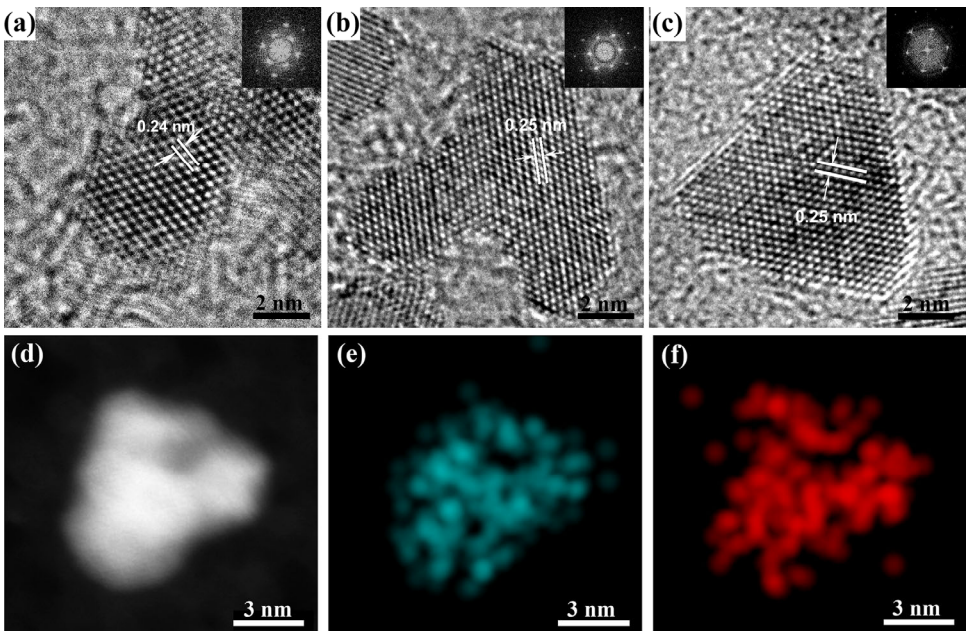

Fig. 2 HRTEM images and their corresponding fast Fourier transform (FFT) patterns of NiO nanocrystals (a), and the resulting alloyed nanocrystals from the 60% $Co(St)_2$ reaction (b) and CoO nanocrystals (c); HADDF image for a single $Co_xNi_{1-x}O$ nanocrystal from the 60% $Co(St)_2$ reaction (d), and the corresponding EDS mapping of Co (e) and Ni (f) elements

reported in several other material systems (Yang *et al.*, 2010; Qiu *et al.*, 2011; Jin *et al.*, 2012; Wang *et al.*, 2013).

The crystalline structures of NiO, $Co_xNi_{1-x}O$, and CoO nanocrystals were investigated by HRTEM and X-ray diffraction (XRD). The FFT patterns of the three representative nanocrystals of NiO, $Co_xNi_{1-x}O$, and CoO nanocrystals, suggest that all oxide nanocrystals show cubic structure (Fig. 2). The interplanar spacing of pure NiO nanocrystals (Fig. 2a) is 0.24 nm, corresponding to the {111} facets of the rock salt structured NiO. Similarly, the interplanar spacing of CoO nanocrystals matches well with the {111} facets of the rock salt structured CoO (0.25 nm) (Fig. 2c). The HADDF-STEM and EDS mapping analyses (Figs. 2d–2f) on a number of alloyed nanocrystals indicate no segregation of cobalt-rich or nickel-rich domains within the nanocrystals. Therefore, we conclude that the Co and Ni elements are homogeneously distributed in the alloyed nanocrystals.

XRD profiles of the $Co_xNi_{1-x}O$ nanocrystals confirm that the crystal structure of all oxide nanocrystals matches the face-centered cubic structure (Fig. 3). The (200) diffraction peaks of the rock salt structure gradually shift from 43.4° (corresponding to NiO) to 42.4° (corresponding to CoO) with the increasing $Co(St)_2$ concentrations in the reagents. Note that the signal-to-noise ratio of Co-rich samples reduces since the mass absorption coefficient of cobalt, 354, is significantly larger than that of nickel, 49.3. The XRD results are consistent with the HRTEM analyses in which the {111} interplanar spacing expands from 0.24 nm to 0.25 nm (Figs. 2a–2c).

The cobalt concentration in the alloyed $Co_xNi_{1-x}O$ nanocrystals was determined by ICP-AES. The results show that the content of cobalt in the alloyed nanocrystals has a linear correlation with the molar ratio of $Co(St)_2$ in the reagents (determination coefficient R^2=0.999 74) (Fig. 4). Therefore, alloyed $Co_xNi_{1-x}O$ nanocrystals with x continuously tuned from 0 to 1 can be realized.

We used XPS to characterize the valence state of Co and Ni ions in the alloyed $Co_xNi_{1-x}O$ nanocrystals. The resulting nanocrystals from the 40% $Co(St)_2$ reaction are chosen as a representative sample (Fig. 5). Binding energy was calibrated using the C 1s photoelectron peak at 284.6 eV. For the convenience of identification, the intensity of the Co 2p spectrum was magnified so that the relative intensity of Co 2p and Ni 2p spectra was irrelevant to the molar ratios of the two cations. In the Ni 2p spectrum, two broad regions at 850–859 eV and 859–869 eV can be

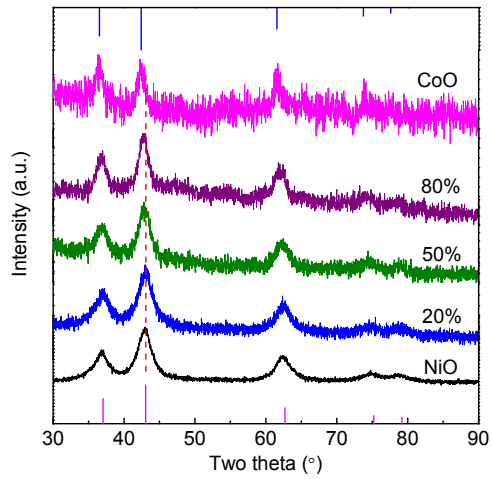

Fig. 3 XRD patterns of $Co_xNi_{1-x}O$ nanocrystals from the reaction with different ratios of $Co(St)_2$

The straight lines at the bottom and at the top represent the diffraction peaks of NiO (PDF no. 47-1049) and CoO (PDF no. 43-1004), respectively

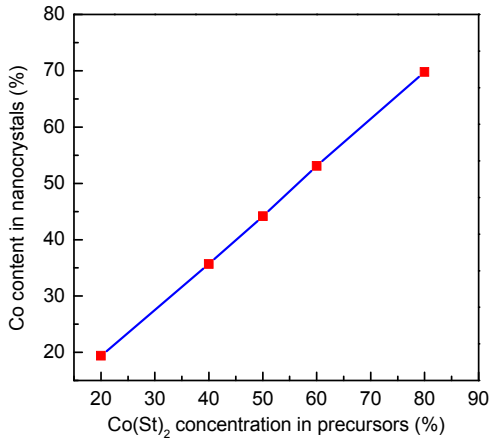

Fig. 4 Co contents in the alloyed $Co_xNi_{1-x}O$ nanocrystals (atomic percent) varied by $Co(St)_2$ concentration in the precursors

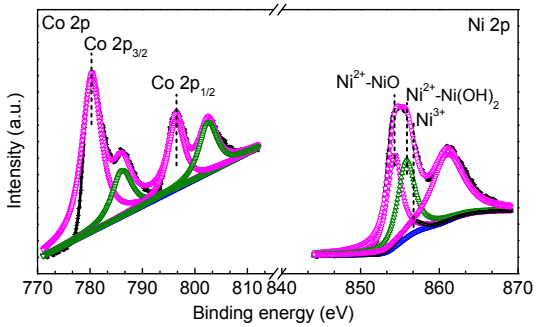

Fig. 5 Ni 2p and Co 2p XPS spectra of the alloyed nanocrystals from 40% $Co(St)_2$ reaction

assigned to Ni $2p_{3/2}$ and the corresponding satellite peak, respectively. The Ni $2p_{3/2}$ peak can be deconvoluted into two peaks centered at 855.8 eV and 853.9 eV, which indicated the existence of $Ni(OH)_2$ and NiO, respectively. The appearance of $Ni(OH)_2$ is due to the absorption of H_2O in the ambient environment (Ratcliff *et al.*, 2011; Peck and Langell, 2012). Trace amount of Ni^{3+} species is also detected in the sample. The interpretation of the Co 2p spectrum is more complicated than that of Ni 2p spectrum because the peaks of both Co $2p_{3/2}$ (~780.1) and Co $2p_{1/2}$ (~796.5 eV) in CoO and Co_3O_4 are very close (Hagelin-Weaver *et al.*, 2004). Yang *et al.* (2007) proposed that the intensity ratio of Co $2p_{1/2}$ satellite peak to main peak was about 0.9 in CoO and about 0.3 in Co_3O_4. This signature can be used to determine the valence state of the Co element. In the case of $Co_xNi_{1-x}O$ nanocrystals from the 40% $Co(St)_2$ reaction, the intensity ratio is 0.82 based on the deconvolution fitting results. Therefore, we suggest that the cobalt ions in the alloyed nanocrystals are Co^{2+}. This suggestion matches the following experiment results that pure CoO nanocrystals were obtained when cobalt (III) acetylacetonate was used as the cobalt precursor in the alcoholysis experiment.

The alloyed $Co_xNi_{1-x}O$ nanocrystals were applied as the hole-transporting layer in the PLED device. A model system of ITO/$Co_xNi_{1-x}O$/MEH-PPV/Ca/Al was used. Fig. 6 shows the current density and luminance of the device, suggesting that the $Co_xNi_{1-x}O$ nanocrystals can act as an effective hole-transporting material.

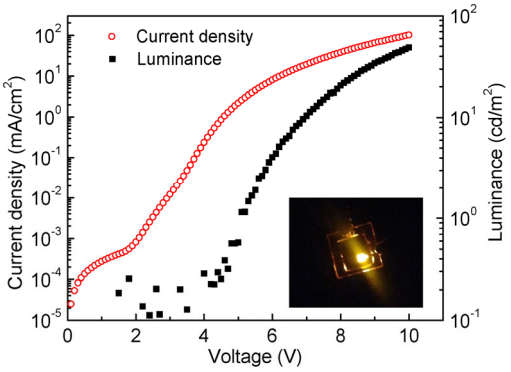

Fig. 6 Current density-voltage and luminance-voltage curves of the MEH-PPV-based PLED using $Co_xNi_{1-x}O$ nanocrystal films as the hole-transporting layer (the inset is the digital image of a PLED device)

4 Conclusions

We demonstrated the syntheses of quality alloyed $Co_xNi_{1-x}O$ ($x \in [0, 1]$) nanocrystals by the protecting-ligand assisted approach. The composition-dependent morphologies and crystal structures of the alloyed $Co_xNi_{1-x}O$ nanocrystals can transform from NiO-dominated to CoO-dominated characteristics. EDS mapping results indicate homogeneous distributions of Ni and Co atoms within the nanocrystals. Our study provides a good example for the syntheses of alloyed oxide nanocrystals with continuously tunable compositions.

References

Choi, S.H., Kang, Y.C., 2014. Ultrafast synthesis of yolk-shell and cubic NiO nanopowders and application in lithium ion batteries. *ACS Applied Materials & Interfaces*, **6**(4): 2312-2316. http://dx.doi.org/10.1021/am404232x

Dai, X.L., Zhang, Z.X., Jin, Y.Z., *et al.*, 2014. Solution-processed, high-performance light-emitting diodes based on quantum dots. *Nature*, **515**(7525):96-99. http://dx.doi.org/10.1038/nature13829

Hagelin-Weaver, H.A.E., Hoflund, G.B., Minahan, D.M., *et al*., 2004. Electron energy loss spectroscopic investigation of Co metal, CoO, and Co_3O_4 before and after Ar^+ bombardment. *Applied Surface Science*, **235**(4):420-448. http://dx.doi.org/10.1016/j.apsusc.2004.02.062

Hüfner, H., 1994. Electronic-structure of NiO and related 3D-transition-metal compounds. *Advances in Physics*, **43**(2):183-356. http://dx.doi.org/10.1080/00018739400101495

Jiang, F., Choy, W.C.H., Li, X.C., *et al*., 2015. Post-treatment-free solution-processed non-stoichiometric NiO_x nanoparticles for efficient hole-transport layers of organic optoelectronic devices. *Advanced Materials*, **27**(18):2930-2937. http://dx.doi.org/10.1002/adma.201405391

Jin, Y.Z., Yi, Q., Zhou, L.M., *et al*., 2012. Synthesis and characterization of ultrathin tin-doped zinc oxide nanowires. *European Journal of Inorganic Chemistry*, **2012**(27):4268-4272. http://dx.doi.org/10.1002/ejic.201200659

Kılıç, Ç., Zunger, A., 2002. N-type doping of oxides by hydrogen. *Applied Physics Letters*, **81**(1):73-75. http://dx.doi.org/10.1063/1.1482783

Kuboon, S., Hu, Y.H., 2011. Study of NiO-CoO and Co_3O_4-Ni_3O_4 solid solutions in multiphase Ni-Co-O systems. *Industrial & Engineering Chemistry Research*, **50**(4):2015-2020. http://dx.doi.org/10.1021/ie101249r

Lang, J.W., Kong, L.B., Wu, W.J., *et al*., 2008. Facile approach to prepare loose-packed NiO nano-flakes materials for supercapacitors. *Chemical Communications*, (35): 4213-4215. http://dx.doi.org/10.1039/b800264a

Liang, X.Y., Yi, Q., Bai, S., *et al*., 2014. Synthesis of unstable colloidal inorganic nanocrystals through the introduction of a protecting ligand. *Nano Letters*, **14**(6):3117-3123. http://dx.doi.org/10.1021/nl501763z

Peck, M.A., Langell, M.A., 2012. Comparison of nanoscaled and bulk NiO structural and environmental characteristics by XRD, XAFS, and XPS. *Chemistry of Materials*, **24**(23):4483-4490. http://dx.doi.org/10.1021/cm300739y

Qiu, H.L., Chen, G.Y., Fan, R.W., *et al*., 2011. Tuning the size and shape of colloidal cerium oxide nanocrystals through lanthanide doping. *Chemical Communications*, **47**(34): 9648-9650. http://dx.doi.org/10.1039/c1cc13707g

Ratcliff, E.L., Meyer, J., Steirer, K.X., *et al*., 2011. Evidence for near-surface NiOOH species in solution-processed NiO_x selective interlayer materials: impact on energetics and the performance of polymer bulk heterojunction photovoltaics. *Chemistry of Materials*, **23**(22):4988-5000. http://dx.doi.org/10.1021/cm202296p

Regulacio, M.D., Han, M.Y., 2010. Composition-tunable alloyed semiconductor nanocrystals. *Accounts of Chemical Research*, **43**(5):621-630. http://dx.doi.org/10.1021/ar900242r

Stiglich, J.J., Cohen, J.B., Whitmore, D.H., 1973a. Interdiffusion in CoO-NiO solid-solutions. *Journal of the American Ceramic Society*, **56**(3):119-126. http://dx.doi.org/10.1111/j.1151-2916.1973.tb15425.x

Stiglich, J.J., Whitmore, D.H., Cohen, J.B., 1973b. Defect structure of NiO-CoO solid solutions. *Journal of the American Ceramic Society*, **56**(4):211-213. http://dx.doi.org/10.1111/j.1151-2916.1973.tb12459.x

Takizawa, K., Hagiwara, A., 2001. Behavior of CoO-NiO solid solution in molten carbonate. *Journal of the Electrochemical Society*, **148**(9):A1034-A1040. http://dx.doi.org/10.1149/1.1390345

Varghese, B., Reddy, M.V., Yanwu, Z., *et al*., 2008. Fabrication of NiO nanowall electrodes for high performance lithium ion battery. *Chemistry of Materials*, **20**(10):3360-3367. http://dx.doi.org/10.1021/cm703512k

Wang, X., Jin, Y.Z., He, H.P., *et al*., 2013. Bandgap engineering and shape control of colloidal $Cd_xZn_{1-x}O$ nanocrystals. *Nanoscale*, **5**(14):6464-6468. http://dx.doi.org/10.1039/c3nr01124k

Wang, Y.F., Zhang, L.J., 2012. Simple synthesis of CoO-NiO-C anode materials for lithium-ion batteries and investigation on its electrochemical performance. *Journal of Power Sources*, **209**:20-29. http://dx.doi.org/10.1016/j.jpowsour.2012.02.074

Wang, Z.Q., Zhang, M., Zhou, J., 2016. Flexible NiO-graphene-carbon fiber mats containing multifunctional

graphene for high stability and high specific capacity lithium-ion storage. *ACS Applied Materials & Interfaces*, **8**(18):11507-11515. http://dx.doi.org/10.1021/acsami.6b01958

White, M.A., Ochsenbein, S.T., Gamelin, D.R., 2008. Colloidal nanocrystals of wurtzite $Zn_{1-x}Co_xO$ ($0\leq x\leq 1$): models of spinodal decomposition in an oxide diluted magnetic semiconductor. *Chemistry of Materials*, **20**(22): 7107-7116. http://dx.doi.org/10.1021/cm802280g

Xiao, S.H., Qu, F.Y., Wu, X., 2016. Ultrathin NiO nanoflakes electrode materials for supercapacitors. *Applied Surface Science*, **360**:8-13. http://dx.doi.org/10.1016/j.apsusc.2015.10.171

Yang, H., Guai, G.H., Guo, C., *et al*., 2011. NiO/Graphene composite for enhanced charge separation and collection in p-type dye sensitized solar cell. *The Journal of Physical Chemistry C*, **115**(24):12209-12215. http://dx.doi.org/10.1021/jp201178a

Yang, H.M., Ouyang, J., Tang, A.D., 2007. Single step synthesis of high-purity CoO nanocrystals. *The Journal of Physical Chemistry B*, **111**(28):8006-8013. http://dx.doi.org/10.1021/jp070711k

Yang, Y.F., Jin, Y.Z., He, H.P., *et al*., 2010. Dopant-induced shape evolution of colloidal nanocrystals: the case of zinc oxide. *Journal of the American Chemical Society*, **132**(38):13381-13394. http://dx.doi.org/10.1021/ja103956p

Yuan, C.Z., Zhang, X.G., Su, L.H., *et al*., 2009. Facile synthesis and self-assembly of hierarchical porous NiO nano/micro spherical superstructures for high performance supercapacitors. *Journal of Materials Chemistry*, **19**(32):5772-5777. http://dx.doi.org/10.1039/b902221j

Zhang, H., Cheng, J.Q., Lin, F., *et al*., 2016. Pinhole-free and surface-nanostructured NiO_x film by room-temperature solution process for high-performance flexible perovskite solar cells with good stability and reproducibility. *ACS Nano*, **10**(1):1503-1511. http://dx.doi.org/10.1021/acsnano.5b07043

Zhang, J., Wang, J.T., Fu, Y.Y., *et al*., 2014. Efficient and stable polymer solar cells with annealing-free solution-processible NiO nanoparticles as anode buffer layers. *Journal of Materials Chemistry C*, **2**(39):8295-8302. http://dx.doi.org/10.1039/C4TC01302F

Zhang, L.P., Mu, J.C., Wang, Z., *et al*., 2016. One-pot synthesis of NiO/C composite nanoparticles as anode materials for lithium-ion batteries. *Journal of Alloys and Compounds*, **671**:60-65. http://dx.doi.org/10.1016/j.jallcom.2016.02.038

Zhou, G., Wang, D.W., Yin, L.C., *et al*., 2012. Oxygen bridges between NiO nanosheets and graphene for improvement of lithium storage. *ACS Nano*, **6**(4):3214-3223. http://dx.doi.org/10.1021/nn300098m

Zhu, Y.F., Liang, X.Y., Jiang, Q., 2008. The effect of alloying on the bandgap energy of nanoscaled semiconductor alloys. *Advanced Functional Materials*, **18**(9):1422-1429. http://dx.doi.org/10.1002/adfm.200700857

中文概要

题　目： **$Co_xNi_{1-x}O$ 合金纳米晶的合成与表征**

目　的： 合成成分连续可调的 $Co_xNi_{1-x}O$ 合金纳米晶，揭示 $Co_xNi_{1-x}O$ 合金纳米晶的形貌和晶体结构随纳米晶中钴离子含量的变化规律以及考察金属离子在合金纳米晶的分布情况。

创新点： 1. 利用金属羧酸盐在有机体系中的醇解反应制备 $Co_xNi_{1-x}O$ 合金纳米晶，其反应温度仅为 270 °C，显著低于文献报道中所使用的温度；2. 成功实现 $Co_xNi_{1-x}O$ 纳米晶成分的调节，发现纳米晶形貌随成分的变化规律；3. 揭示了金属离子在合金纳米晶中的均匀分布。

方　法： 1. 在硬脂酸锂的“配体保护”作用下，利用金属羧酸盐的醇解反应制备 $Co_xNi_{1-x}O$ 合金纳米晶；2. 利用透射电子显微镜、X 射线衍射、原子发射光谱和 X 射线光电子等手段研究 $Co_xNi_{1-x}O$ 合金纳米晶的形貌、晶体结构、成分和金属离子价态等信息。

结　论： 1. 成功地制备出高质量的 $Co_xNi_{1-x}O$ ($x\in[0, 1]$)合金纳米晶；2. 发现 $Co_xNi_{1-x}O$ 合金纳米晶的形貌和晶体结构随纳米晶中钴离子浓度的提高呈现出由 NiO 特征过渡到 CoO 特征的趋势；3. 对单颗 $Co_xNi_{1-x}O$ 合金纳米晶的元素扫描揭示了金属离子在纳米晶中的均匀分布。

关键词： 合金化；氧化镍；氧化钴；胶体纳米晶